STRUCTURAL SCIENCE
CRYSTAL ENGINEERING
MATERIALS

ISSN 2052-5206

Polymorphism of $Pb_5(PO_4)_3OH_\delta$ within the LK-99 mixture

Mingyu Xu, Haozhe Wang, Cameron Vojvodin, Jayasubba Reddy Yarava, Tuo Wang and Weiwei Xie*

Department of Chemistry, Michigan State University, East Lansing, MI 48824, USA. *Correspondence e-mail: xieweiwe@msu.edu

Received 11 March 2024
Accepted 14 October 2024

Edited by C. M. Reddy, IISER Kolkata, India

Keywords: orthorhombic apatite; superconductivity; LK-99.

CCDC reference: 2391128

Supporting information: this article has supporting information at journals.iucr.org/b

During the synthetic exploration targeting the polycrystalline compound LK-99, an unexpected phase, $Pb_5(PO_4)_3OH_\delta$, was identified as a byproduct. We elucidated the composition of this compound through single-crystal X-ray diffraction analysis. Subsequent synthesis of the target compounds was achieved via high-temperature solid-state pellet reactions. The newly identified $Pb_5(PO_4)_3OH_\delta$ has an orthorhombic crystal structure with space group *Pnma*, representing a unique structure differing from the hexagonal apatite phases of $Pb_{10}(PO_4)_6O$ and $Pb_5(PO_4)_3OH$. Comprehensive temperature- and magnetic-field-dependent magnetization studies unveiled a temperature-independent magnetic characteristic of $Pb_5(PO_4)_3OH_\delta$. Solid-state nuclear magnetic resonance spectroscopy was employed to decipher the origins of the phase stability and confirm the presence of hydrogen atoms in $Pb_5(PO_4)_3OH_\delta$. These investigations revealed the presence of protonated oxygen sites, in addition to the interstitial water molecules within the structure, which may play critical roles in stabilizing the orthorhombic phase.

1. Introduction

After the claim of the discovery of an ambient-pressure room-temperature superconductor (T_c > 400 K) LK-99, $(Pb_{10-x}Cu_x)(PO_4)_6O$ (Lee, Kim & Kwon, 2023), with a subsequent report of a levitation experiment at room temperature indicating strong diamagnetic signals (Lee, Kim, Kim *et al.*, 2023), LK-99 has garnered unprecedented attention. Despite numerous attempts by various research groups to replicate and verify the superconductivity of LK-99 (Zhu *et al.*, 2023; Timokhin *et al.*, 2023; Kumar *et al.*, 2023; Wu *et al.*, 2023; Hou *et al.*, 2023), increasing experimental evidence has begun to cast doubt on its superconducting nature (Garisto, 2023).

In the quest to unravel the mysteries of LK-99's superconductivity, our investigation has led to the discovery of several new phases. Among these, the novel structure of hydroxylpyromorphite, $Pb_5(PO_4)_3OH_\delta$, stands out and is different from the conventional hexagonal phase known for $Pb_{10}(PO_4)_6O$ (Brückner *et al.*, 1995; Kim *et al.*, 1997; Barinova *et al.*, 1998). The compound $Pb_{10}(PO_4)_6O$ has been termed oxypyromorphite, a nomenclature that underscores its structural resemblance to pyromorphite, $Pb_5(PO_4)_3Cl$, and hydroxylpyromorphite, $Pb_5(PO_4)_3(OH)$, which adopts an apatite-like hexagonal structure, wherein O^{2-} anions substitute for the halide ions typically found in apatite structures. This substitution suggests the presence of vacancies at some halide sites, in contrast to the original proposition of a $(Pb^{2+})_9(Pb^{4+})(PO_4)_6O_2$ formula (Ito, 1968), which would negate the need for such vacancies. However, further studies

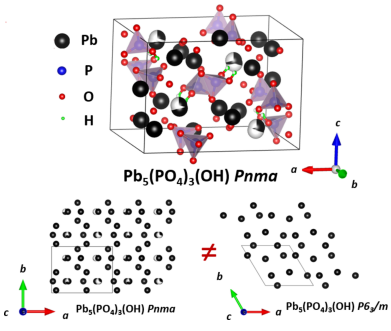

confirmed the absence of Pb^{4+} cations in oxypyromorphite (Merker *et al.*, 1970). Despite its intriguing properties, detailed crystal structure analysis of oxypyromorphite has yet to be carried out. In addition, the lead-based compounds $Pb_4O(PO_4)_2$, $Pb_8O_5(PO_4)_2$ and $Pb_{10}(PO_4)_6O$ have been studied for several decades (Yang *et al.*, 2001; Brixner & Foris, 1973; Krivovichev & Burns, 2003). The ferro-elastic $Pb_8O_5(PO_4)_2$ and its vanadium analog $Pb_8O_5(VO_4)_2$ (Dudnik & Kolesov, 1980; Kiosse *et al.*, 1982) have also been discovered. Although X-ray and optical analyses on the single crystals of these compounds have been conducted, the crystal structures of both remain unresolved.

In this study, we present a synthetic strategy for the new $Pb_5(PO_4)_3OH_\delta$ compound using a high-temperature solid-state pellet reaction. Millimetre-sized single crystals were obtained from the reaction. Single-crystal and powder X-ray diffraction (XRD) experiments were conducted to determine the crystal structure and confirm the phase information. Accordingly, $Pb_5(PO_4)_3OH_\delta$ was found to crystallize in the orthorhombic crystal system with the space group *Pnma*. Different from the hexagonal apatite phase $Pb_{10}(PO_4)_6O$ with the balanced charge of $(Pb^{2+})_{10}(PO_4{}^{3-})_6O^{2-}$, the compound of $Pb_5(PO_4)_3O$ cannot be charge-balanced with the sole existence of Pb^{2+} and full occupancies on all atomic sites. To confirm the existence of a proton (H^+) to balance the charge in $Pb_5(PO_4)_3OH_\delta$, high-magnetic-field (800 MHz or 18.8 T) solid-state nuclear magnetic resonance (NMR) spectroscopy was used to determine the chemical environments of proton sites and the presence of water molecules in the system.

2. Synthesis and experimental methods

2.1. Chemical synthesis

$Pb_5(PO_4)_3OH_\delta$ crystals were synthesized in two steps. The first step was synthesis of the precursors. The mixture of PbO (99.3%, BAKER ANALYZED) and $PbSO_4$ (99.1%, BAKER ANALYZED) was heated under a vacuum for 24 h with 1:1 mole ratio. After the reaction, we obtained the $Pb_2(SO_4)O$ precursor with $Pb_3(SO_4)O_2$ (∼1.5 at.%]) impurity. Another precursor is Cu_3P, obtained by heating Cu powder (99.9%, Alfa Aesar) and P powder (99%, Beantown Chemical) for 48 h at 550°C under vacuum. The molar ratio of Cu and P was 3:1 and the powder XRD results of the two precursors are shown in the supporting information (Figs. S1a and S1b). The second step was mixing $Pb_2(SO_4)O$ and Cu_3P in the ratio 5:3, remaining at 925°C for 20 h. Millimetre-size single crystals of $Pb_5(PO_4)_3OH_\delta$ were obtained. All the reaction products were powder pressed using a 0.25 inch (internal diameter) dry pellet pressing die made of carbon steel. A 2 ml alumina cylindrical crucible held the pressed pellet before it was sealed in a fused silica tube under vacuum with around 30 mTorr pressure. After the solid-state reaction, transparent single-crystalline samples can easily be identified on the bottom pellet, which can be separated from black-colored polycrystalline chunks and copper-colored solidified drops on the surface of the black chunks. The rest of the measurements were done using the single crystals separated mechanically from the mixture.

Table 1
Experimental details.

Values in parentheses are the estimated standard deviation from refinement.

Chemical formula	$Pb_5(PO_4)_3OH$
Formula weight (g mol^{-1})	1337.87
Space group	*Pnma*
Unit-cell dimensions (Å)	a = 13.5137 (4), b = 10.2904 (4), c = 9.3838 (3)
Volume (Å^3)	1304.93 (7)
Z, Z'	4, 0.5
Density (calculated) (g cm^{-3})	6.810
Absorption coefficient μ (mm^{-1})	64.725
Crystal size (mm)	0.076 × 0.056 × 0.049
F(000)	2240
Data collection	
2θ range (°)	5.286–82.472
No. of reflections collected	48595
No. of independent reflections	4458
R_{int}	0.1257
Refinement method	Full-matrix least-squares on F^2
No. of data, restraints, parameters	4458, 0, 114
Final R indices	R_1 [$I > 2\sigma(I)$] = 0.0402; wR_2 [$I > 2\sigma(I)$] = 0.0681 R_1 (all) = 0.0811; wR_2 (all) = 0.0758
$\Delta\rho_{max}$, $\Delta\rho_{min}$ (e Å^{-3})	+3.79 and −5.99
RMS deviation from mean (e Å^{-3})	0.511
Goodness-of-fit on F^2	1.047

2.2. Structure determination and phase analysis

$Pb_5(PO_4)_3OH_\delta$ forms transparent, rod-like, brittle single crystals. A single crystal was selected, mounted on a nylon loop with Paratone oil and measured using an XtalLAB Synergy, Dualflex, Hypix single-crystal X-ray diffractometer. Data were collected using ω scans with Mo $K\alpha$ radiation (λ = 0.71073 Å) and Ag $K\alpha$ radiation (λ = 0.56087 Å), a micro-focus sealed X-ray tube, 65 kV, 0.67 mA. The total number of runs and images was based on the strategy calculation from the *CrysAlisPro* (Rigaku OD, 2017) program. Data reduction was performed with correction for Lorentz polarization. A numerical absorption correction was applied based on Gaussian integration over a multifaceted crystal model (Parkin *et al.*, 1995). Empirical absorption correction used spherical harmonics, implemented in the *SCALE3 ABSPACK* scaling algorithm (Walker & Stuart, 1983). The structure was solved and refined using the *SHELXTL* software package (Sheldrick, 2015*a*, Sheldrick, 2015*b*). Tables 1 and 2 show the results of the single-crystal XRD. For the powder XRD measurements, single crystals were ground in an agate mortar and pestle, and the powder placed onto the 20 × 20 × 0.5 mm Rigaku Square groove. Powder XRD measurements were carried out using a Rigaku MiniFlex powder diffractometer in Bragg–Brentano geometry with Cu $K\alpha$ radiation (λ = 1.5406 Å). Room-temperature measurements were performed with a step size of 0.01° at a scan speed of 0.5° per minute over a Bragg angle (2θ) range of 10–90°. *GSAS II* (Toby & Von Dreele, 2013) was used to perform the Rietveld refinement and analyze phase information.

Table 2
Atomic coordinates and equivalent isotropic atomic displacement parameters (Å^2) of $Pb_5(PO_4)_3OH$.

U_{eq} is one-third of the trace of the orthogonalized U_{ij} tensor. Values in parentheses are the estimated standard deviation from refinement.

Atoms	Wyckoff site	x	y	z	Occ.	U_{eq}
Pb1	8*d*	0.07377 (2)	0.55577 (2)	0.29630 (2)	1	0.019 (1)
Pb2	4*c*	0.02043 (2)	0.75	−0.02843 (3)	1	0.017 (1)
Pb3	4*c*	0.23350 (3)	0.75	−0.30356 (4)	1	0.025 (1)
Pb4	4*c*	0.2750 (2)	0.75	0.1556 (2)	0.71	0.0285 (2)
Pb5	4*c*	0.2703 (5)	0.75	0.1277 (6)	0.29	0.05 (1)
P1	8*d*	−0.1631 (1)	0.5324 (1)	0.07074 (1)	1	0.0123 (2)
P2	4*c*	0.0030 (2)	0.75	−0.4252 (2)	1	0.0153 (4)
O1	4*c*	−0.0913 (6)	0.75	−0.34610 (8)	1	0.0402 (2)
O2	4*c*	−0.071 (5)	0.75	0.4179 (7)	1	0.0260 (1)
O3	4*c*	0.1089 (4)	0.75	0.1753 (5)	1	0.013 (1)
O4	8*d*	−0.1751 (4)	0.3859 (4)	0.0955 (4)	1	0.0248 (9)
O5	8*d*	−0.1685 (4)	0.5588 (5)	−0.0902 (5)	1	0.030 (1)
O6	8*d*	−0.0618 (4)	0.5794 (5)	0.1249 (6)	1	0.031 (1)
O7	8*d*	−0.2451 (4)	0.6053 (5)	0.1488 (6)	1	0.033 (1)
O8	8*d*	0.0635 (4)	0.8677 (5)	−0.3915 (7)	1	0.041 (1)
H	8*d*	0.0993	0.85244	−0.322954	0.5	0.061

2.3. Solid-state NMR spectroscopy for detecting protons

^{1}H solid-state NMR experiments were conducted on a Bruker NEO spectrometer with a narrow-bore magnet with B_0 = 18.8 T [ν_0(^{1}H) = 800 MHz] at room temperature (298 K). Spectra were acquired using a Phoenix NMR 1.6 mm HXY magic-angle spinning (MAS) probe with samples packed into 1.6 mm (outer diameter) zirconia rotors. The MAS frequency was set to 8 kHz. ^{1}H chemical shifts were referenced to alanine (δ_{iso} = 1.38 p.p.m.) as a secondary reference with respect to tetramethylsilane (δ_{iso} = 0 p.p.m.). All ^{1}H spectra were acquired using a rotor-synchronized Hahn echo (90°–τ–180° acquisition) with 2.5 µs (100 kHz) π/2 pulses, an interpulse delay (τ) of 500 µs and a recycle delay of 2 s (see Table S1 for further details). Spectra were processed in *TopSpin 4.1* (Bruker), and simulations of all spectra were prepared using *ssNake* v1.3 (van Meerten *et al.*, 2019).

2.4. Magnetic measurements

Temperature- and magnetic-field-dependent DC and vibrating sample magnetometry (VSM) magnetization data were collected using a Quantum Design Magnetic Property Measurement System (MPMS3). Temperature- and magnetic-field-dependent DC magnetization measurements were taken on the powder sample loaded in the powder sample holder and put into a brass half-tube sample holder. In VSM measurements, a peak amplitude of 5 mm and an average of 2 s were used. An empty powder sample holder was measured under the same conditions to estimate the background to be subtracted from the measurements.

3. Results and discussion

The crystal structure of $Pb_5(PO_4)_3OH_\delta$ exhibits similarities to apatite-like lead compounds, including pyromorphite [$Pb_5(PO_4)_3Cl$], hydroxylapatite [$Pb_5(PO_4)_3(OH)$] and the LK-99 precursor, $Pb_{10}(PO_4)_6O$. Previous determinations of hydroxylapatite's structure, through neutron and X-ray powder diffraction analysis, identified the OH group positioned at the 4*e* Wyckoff site with a 0.5 site occupation factor (Kim *et al.*, 1997). In contrast, Barinova *et al.*'s refinement using single-crystal diffraction data located the OH group at the 2*b* site, indicating full occupancy – a characteristic more aligned with the halide ion positions in pyromorphite-like compounds ($Pb_5(PO_4)_3X$, where X = F, Cl (Barinova *et al.*, 1998). The structural framework of $Pb_{10}(PO_4)_6O$ mirrors that of hydroxylapatite, with the O4 atom situated at the 4*e* site, albeit with a reduced occupation factor of 0.25. Our investigation into a single crystal of $Pb_5(PO_4)_3OH_\delta$ revealed a deviation from the expected hexagonal structure to an

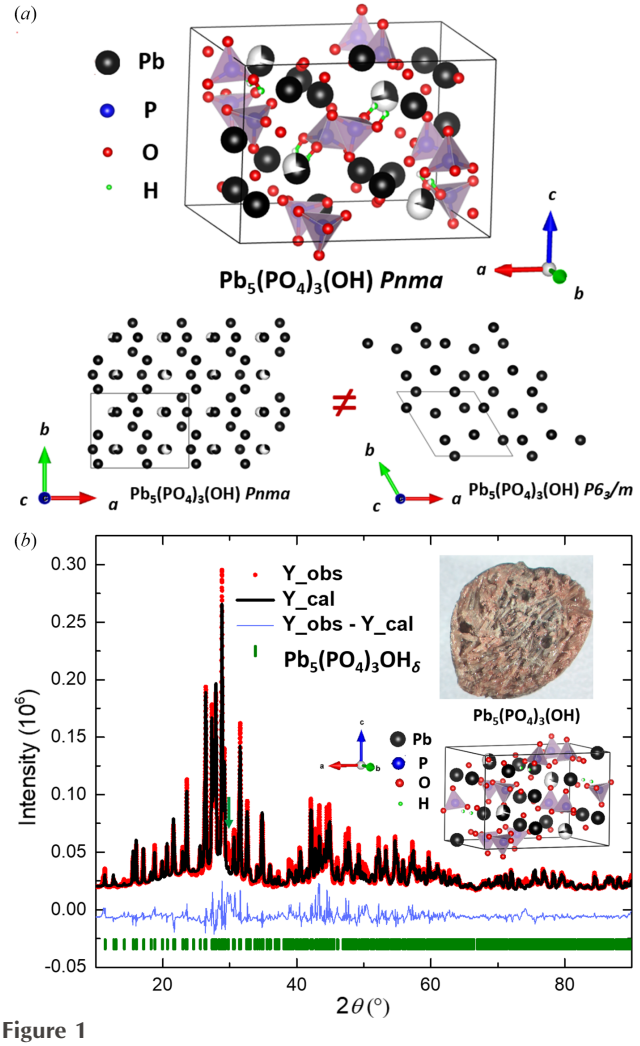

Figure 1
The crystal structure and the powder XRD data of $Pb_5(PO_4)_3OH_\delta$. (*a*) shows the crystal structure of $Pb_5(PO_4)_3(OH)$ from single-crystal XRD and a comparison of Pb atom distribution between the orthorhombic and hexagonal structures. (*b*) Powder XRD data of $Pb_5(PO_4)_3OH_\delta$ from in-laboratory diffraction measurements. The experimental data are plotted as red dots. The black line gives the Rietveld refinement. The blue line indicates the corresponding residual pattern (difference between observed and calculated patterns). Bars give $Pb_5(PO_4)_3OH_\delta$ peak positions from single-crystal XRD measurement. The green arrow indicates the peak from an impurity. On the upper right of the figure, a picture of the crystals is shown; the size of the chunk is about 5 mm.

orthorhombic *Pnma* space group, attributed to lattice parameter distortions, as shown in Fig. 1(*a*). The hydrogen atoms were refined with half occupancy at the 8*d* sites. However, considering the limitations of XRD in accurately detecting hydrogen positions, we employed high-field ^{1}H solid-state NMR (ssNMR) to further elucidate the hydrogen occupancies, providing a more comprehensive understanding of the structural intricacies of $Pb_5(PO_4)_3OH_\delta$. To ascertain the phase purity and facilitate the investigation of its physical properties, powder XRD analysis was performed, with the results presented in Fig. 1(*b*). The data were refined using Rietveld refinement, and the green peak suggests a peak from a minor impurity phase.

The ^{1}H ssNMR spectrum features six underlying peaks with their isotropic chemical shifts (δ_{iso}) ranging from 0.8 to 5.2 p.p.m. in a 1:1.2:2.1:2.7:10.4:3.6 ratio from left to right (Fig. 2 and Table 3). This is surprising since the solved single-crystal XRD structure only includes one hydrogen position, while the NMR data indicate a far more complex ^{1}H environment. It is not unusual for ssNMR to detect additional structural features that are invisible to XRD techniques (Morris *et al.*, 2017; Zhang *et al.*, 2022; Inukai *et al.*, 2016; Corlett *et al.*, 2019; Li *et al.*, 2013; Serrano-Sevillano *et al.*, 2019). A few possible explanations for these hydrogen resonances are: (i) structural defects in the sample where the phosphate ion reacts with atmospheric water, (ii) water being incorporated into the structure, either occupying vacancies in the octahedral or tetrahedral holes in the crystal structure and/or (iii) atmospheric water being bound to the lead as a ligand.

Since only a single spectrum for $Pb_5(PO_4)_3OH_\delta$ was acquired with no internal reference, only approximate estimation of the amount of hydrogen in the sample is possible. Precise quantification would require a low radiofrequency pulse, a different pulse sequence (*i.e.* Bloch decay), accurate site assignments of all hydrogen atoms and a series of standards to construct a calibration curve (Bharti & Roy, 2012; Pauli *et al.*, 2012; Giraudeau, 2017; Holzgrabe, 2010; Pauli *et al.*, 2015). Hence, we are limited to approximately quantifying the $Pb_5(PO_4)_3OH_\delta$ spectrum relative to another ^{1}H NMR spectrum of a known sample. First, a ^{1}H spectrum of alanine with the exact same experimental parameters as $Pb_5(PO_4)_3OH_\delta$ was acquired using a sufficiently long recycle delay (in this case, 2 s) to completely re-equilibrate the magnetization before the next scan. Second, a Hahn echo with a long interpulse delay (in this case, 500 µs) was used for these experiments in order to eliminate the broad ^{1}H background signal from the probe to allow for easier quantification of the spectra. It has been shown that the relative quantification of NMR spectra of two compounds is possible using the following equation (Malz & Jancke, 2005):

$$\frac{n_x}{n_y} = \frac{I_x}{I_y} \times \frac{N_y}{N_x}, \tag{1}$$

where n_x/n_y is the molar ratio, I_x/I_y is the total integrated intensity ratio and N is the number of nuclei corresponding to the resonance line. Using the total integrated intensities from a spectrum of alanine and $Pb_5(PO_4)_3OH_\delta$, we are able to write equation (2) for approximately quantifying the spectrum as

$$m = \frac{I_{\text{unknown}}}{I_{\text{alanine}}} \times \left(\frac{m_{\text{alanine}}}{M_{\text{alanine}}} \times S_{\text{alanine}} \right), \tag{2}$$

where I is the total integrated intensity of the spectrum, M is the molecular weight, m is the mass of the sample packed in the NMR rotor and S is the number of moles of hydrogen in the sample. Using equation (2), we were able to estimate the amount of hydrogen in $Pb_5(PO_4)_3OH_\delta$ to be approximately 82.5 µg or 1.15 wt%.

While Fig. 1(*b*) depicted the primary phase of the transparent single crystal, $Pb_5(PO_4)_3OH_\delta$, the data also suggested the presence of minor impurity phases within the sample. Single-crystal and powder XRD analyses have identified Cu_2S as the predominant impurity. Prior to evaluating the magnetization data, it is essential to consider the potential magnetic contributions from Cu_2S impurities. If Cu_2S were to significantly influence the magnetic behavior, one might expect to observe a β-to-γ phase transition around 370 K in resistivity, heat capacity and magnetic susceptibility measurements (Zhu *et al.*, 2023). VSM measurements, conducted without background subtraction across a temperature range of 1.8 to 400 K and presented in Fig. 3, do not reveal any magnetic transition

Table 3
Isotropic chemical shifts (δ_{iso}) and percentages of ^{1}H resonances from ssNMR.

	Peak					
Parameter	*a*	*b*	*c*	*d*	*e*	*f*
δ_{iso} (p.p.m.)	5.2	2.2	2.0	1.5	1.3	0.8
Percentage (%)	5	6	10	13	50	17

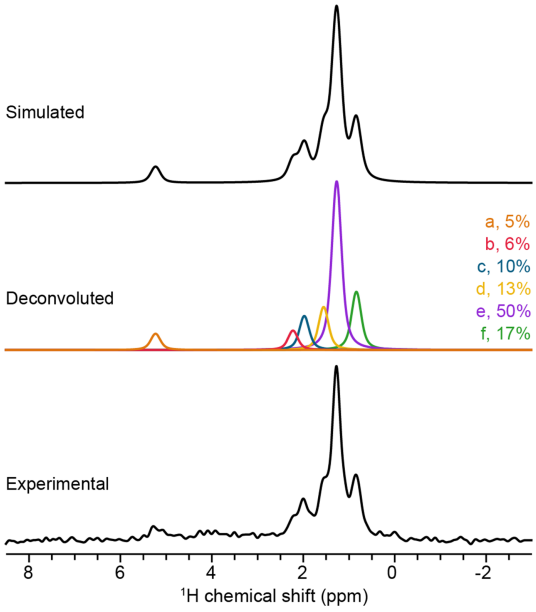

Figure 2
^{1}H MAS solid-state NMR analysis of $Pb_5(PO_4)_3OH_\delta$. Experimental ^{1}H MAS NMR of $Pb_5(PO_4)_3OH_\delta$ is shown in blue, with corresponding analytical simulations in black, and deconvolution of the simulation is shown in color. Six ^{1}H resonances are color-coded and labeled as *a*–*f*, with their relative intensity percentages provided.

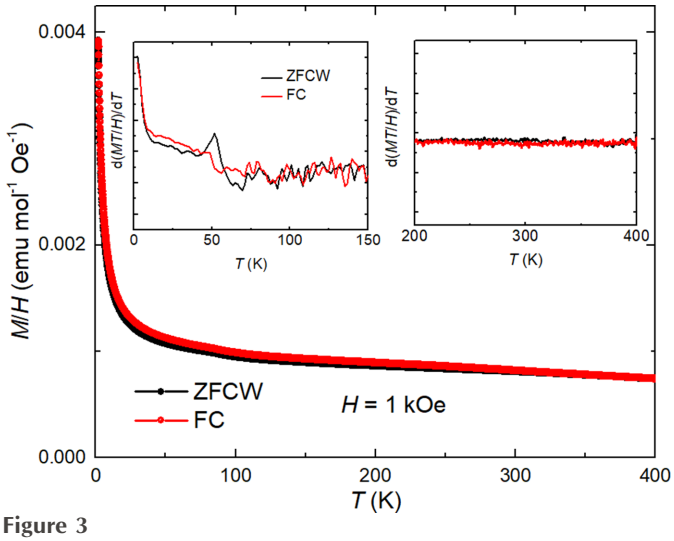

Figure 3
Temperature-dependent magnetization of $Pb_5(PO_4)_3OH_\delta$. ZFCW and FC magnetization as a function of temperature is given by VSM in the range of 1.8–400 K with a field of 1 kOe. The left inset shows d(MT/H)/dT as a function of temperature in the low-temperature range. The right inset shows the derivative of d(MT/H)/dT in the high-temperature range.

near 370 K. The large positive magnetization is also different from previous work (Zhu *et al.*, 2023). The presence of undetected impurity phases, a common occurrence in the solid-state synthesis of LK-99, cannot be overlooked. Fig. 3 presents the findings from temperature-dependent magnetization investigations, conducted under identical experimental conditions to those applied to an empty sample holder to guarantee precision. The magnetization profiles depicted in Fig. 3, obtained through zero-field-cooled-warming (ZFCW) and field-cooled (FC) methods, exhibit distinctive Curie–Weiss-like behavior fitting is shown in Figs. S2a and S2b). A significant deviation between the ZFCW and FC data is evident around 50 K, where a kink-like anomaly, potentially arising from oxygen trapped in the measured sample, is identified in the ZFCW magnetization trajectory. This anomaly is accentuated in the derivative d(MT/H)/dT plot, prominently featured in the inset at the upper-left corner of the figure, further emphasizing its significance. The field-dependent magnetization is also shown in Fig. S3b.

In conclusion, the orthorhombic phase of $Pb_5(PO_4)_3OH_\delta$ was successfully synthesized via solid-state reaction techniques with the objective of creating LK-99. The determination of the phase composition and crystal structure of the product was achieved through an integrated approach, utilizing both single-crystal and powder X-ray diffraction analyses, complemented by solid-state NMR spectroscopy.

Funding information

The following funding is acknowledged: US Department of Energy (grant No. DE-SC0023648).

References

Barinova, A. V., Bonin, M., Pushcharovskii, D. Y., Rastsvetaeva, R. K., Schenk, K. & Dimitrova, O. V. (1998). *Crystallogr. Rep.* **2**, 189.
Bharti, S. K. & Roy, R. (2012). *TrAC Trends Anal. Chem.* **35**, 5–26.
Brixner, L. H. & Foris, C. M. (1973). *J. Solid State Chem.* **7**, 149–154.
Brückner, S., Lusvardi, G., Menabue, L. & Saladini, M. (1995). *Inorg. Chim. Acta*, **236**, 209–212.
Corlett, E. K., Blade, H., Hughes, L. P., Sidebottom, P. J., Walker, D., Walton, R. I. & Brown, S. P. (2019). *CrystEngComm*, **21**, 3502–3516.
Dudnik, E. F. & Kolesov, I. S. (1980). *Sov. Phys. Solid State*, **22**, 700.
Garisto, D. (2023). *Nature*, **620**, 705–706.
Giraudeau, P. (2017). *Magn. Reson. Chem.* **55**, 61–69.
Holzgrabe, U. (2010). *Prog. Nucl. Magn. Reson. Spectrosc.* **57**, 229–240.
Hou, Q., Wei, W., Zhou, X., Sun, Y. & Shi, Z. (2023). *arXiv*:2308.01192.
Inukai, M., Horike, S., Itakura, T., Shinozaki, R., Ogiwara, N., Umeyama, D., Nagarkar, S. S., Nishiyama, Y., Malon, M., Hayashi, A., Ohhara, T., Kiyanagi, R. & Kitagawa, S. (2016). *J. Am. Chem. Soc.* **138**, 8505–8511.
Ito, J. (1968). *Am. Mineral.* **53**, 890.
Kim, J. Y., Hunter, B. A., Fenton, R. R. & Kennedy, B. J. (1997). *Aust. J. Chem.* **50**, 1061.
Kiosse, G. A., Dudnik, E. F., Sushko, S. A. & Kolesov, I. S. (1982). *Sov. Phys. Crystallogr.* **27**, 713.
Krivovichev, S. V. & Burns, P. C. (2003). *Z. Kristallogr. Cryst. Mater.* **218**, 357.
Kumar, K., Karn, N. K., Kumar, Y. & Awana, V. P. S. (2023). *arXiv*:2308.03544.
Lee, S., Kim, J., Kim, H.-T., Im, S., An, S. & Auh, K. H. (2023). *arXiv*:2307.12037.
Lee, S., Kim, J.-H. & Kwon, Y.-W. (2023). *arXiv*:2307.12008.
Li, Z., Miyoshi, T., Sen, M. K., Koga, T., Otsubo, A. & Kamimura, A. (2013). *Macromolecules*, **46**, 6507–6519.
Malz, F. & Jancke, H. (2005). *J. Pharm. Biomed. Anal.* **38**, 813–823.
Meerten, S. G. J. van, Franssen, W. M. J. & Kentgens, A. P. M. (2019). *J. Magn. Reson.* **301**, 56–66.
Merker, L., Engel, G., Wondratschek, H. & Ito, J. (1970). *Am. Mineral.* **55**, 1435.
Morris, S. A., Bignami, G. P. M., Tian, Y., Navarro, M., Firth, D. S., Čejka, J., Wheatley, P. S., Dawson, D. M., Slawinski, W. A., Wragg, D. S., Morris, R. E. & Ashbrook, S. E. (2017). *Nat. Chem.* **9**, 1012–1018.
Parkin, S., Moezzi, B. & Hope, H. (1995). *J. Appl. Cryst.* **28**, 53–56.
Pauli, G. F., Chen, S. N., Simmler, C., Lankin, D. C., Gödecke, T., Jaki, B. U., Friesen, J. B., McAlpine, J. B. & Napolitano, J. G. (2015). *J. Med. Chem.* **58**, 9061.
Pauli, G. F. T., Gödecke, T., Jaki, B. U. & Lankin, D. C. (2012). *J. Nat. Prod.* **75**, 834–851.
Rigaku OD (2017). *CrysAlis PRO*. Rigaku Oxford Diffraction, Yarnton, UK.
Serrano-Sevillano, J., Carlier, D., Saracibar, A., Lopez del Amo, J. M. & Casas-Cabanas, M. (2019). *Inorg. Chem.* **58**, 8347–8356.
Sheldrick, G. M. (2015*a*). *Acta Cryst.* A**71**, 3–8.
Sheldrick, G. M. (2015*b*). *Acta Cryst.* C**71**, 3–8.
Timokhin, I., Chen, C., Wang, Z., Yang, Q. & Mishchenko, A. (2023). *arXiv*:2308.03823.
Toby, B. H. & Von Dreele, R. B. (2013). *J. Appl. Cryst.* **46**, 544–549.
Walker, N. & Stuart, D. (1983). *Acta Cryst.* A**39**, 158–166.
Wu, H., Yang, L., Xiao, B. & Chang, H. (2023). *arXiv*:2308.01516.
Yang, J., Mosby, D. E., Casteel, S. W. & Blanchar, R. W. (2001). *Environ. Sci. Technol.* **35**, 3553–3559.
Zhang, W., Chen, S., Terskikh, V. V., Lucier, B. E. G. & Huang, Y. (2022). *Solid State Nucl. Magn. Reson.* **119**, 101793.
Zhu, S., Wu, W., Li, Z. & Luo, J. (2023). *Matter*, **6**, 4401–4407.